CLEO CONF 96-8
ICHEP96 PA05-079

Measurement of the Form Factors for $\bar{B}^0 \to D^{*+}\ell^-\bar{\nu}$ and $B^- \to D^{*0}\ell^-\bar{\nu}$

CLEO Collaboration

(July 18, 1996)

Abstract

Using a sample of 2.6×10^6 $\Upsilon(4S) \to B\bar{B}$ events collected with the CLEO II detector at the Cornell Electron Storage Ring, we have measured the form factors for the decays $\bar{B}^0 \to D^{*+}\ell^-\bar{\nu}$ and $B^- \to D^{*0}\ell^-\bar{\nu}$. In the mode $\bar{B}^0 \to D^{*+}\ell^-\bar{\nu}$, we perform a three-parameter fit to the joint distribution of four kinematic variables to obtain the form factor ratios $R_1 = 1.18 \pm 0.30 \pm 0.12$ and $R_2 = 0.71 \pm 0.22 \pm 0.07$, and the form-factor slope $\rho^2_{A_1} = 0.91 \pm 0.15 \pm 0.06$, which is closely related to the slope of the Isgur-Wise function. A similar fit in the mode $B^- \to D^{*0}\ell^-\bar{\nu}$ yields the preliminary result $R_1 = 1.46 \pm 0.49 \pm 0.22$, $R_2 = 0.82 \pm 0.33 \pm 0.11$, and $\rho^2_{A_1} = 0.98 \pm 0.22 \pm 0.07$, while a fit to both modes together gives $R_1 = 1.24 \pm 0.26 \pm 0.12$, $R_2 = 0.72 \pm 0.18 \pm 0.07$, and $\rho^2_{A_1} = 0.92 \pm 0.12 \pm 0.06$. The form factor ratios are consistent with predicted corrections to the heavy-quark symmetry limit $R_1 = R_2 = 1$.

A. Anastassov,[1] S. Blinov,[1,*] J. E. Duboscq,[1] R. Fulton,[1] D. Fujino,[1] K. K. Gan,[1] T. Hart,[1] K. Honscheid,[1] H. Kagan,[1] R. Kass,[1] J. Lee,[1] M. Sung,[1] A. Undrus,[1,*] R. Wanke,[1] A. Wolf,[1] M. M. Zoeller,[1] B. Nemati,[2] S. J. Richichi,[2] W. R. Ross,[2] P. Skubic,[2] M. Wood,[2] M. Bishai,[3] J. Fast,[3] E. Gerndt,[3] J. W. Hinson,[3] D. H. Miller,[3] E. I. Shibata,[3] I. P. J. Shipsey,[3] M. Yurko,[3] L. Gibbons,[4] S. D. Johnson,[4] Y. Kwon,[4] S. Roberts,[4] E. H. Thorndike,[4] C. P. Jessop,[5] K. Lingel,[5] H. Marsiske,[5] M. L. Perl,[5] S. F. Schaffner,[5] D. Ugolini,[5] R. Wang,[5] X. Zhou,[5] T. E. Coan,[6] V. Fadeyev,[6] I. Korolkov,[6] Y. Maravin,[6] I. Narsky,[6] V. Shelkov,[6] R. Stroynowski,[6] J. Staeck,[6] I. Volobouev,[6] J. Ye,[6] M. Artuso,[7] A. Efimov,[7] M. Gao,[7] M. Goldberg,[7] R. Greene,[7] F. Frasconi,[7] D. He,[7] S. Kopp,[7] G. C. Moneti,[7] R. Mountain,[7] Y. Mukhin,[7] S. Schuh,[7] T. Skwarnicki,[7] S. Stone,[7] X. Xing,[7] J. Bartelt,[8] S. E. Csorna,[8] V. Jain,[8] S. Marka,[8] A. Freyberger,[9] R. Godang,[9] D. Gibaut,[9] K. Kinoshita,[9] I. C. Lai,[9] P. Pomianowski,[9] S. Schrenk,[9] G. Bonvicini,[10] D. Cinabro,[10] L. Perera,[10] B. Barish,[11] M. Chadha,[11] S. Chan,[11] G. Eigen,[11] J. S. Miller,[11] C. O'Grady,[11] M. Schmidtler,[11] J. Urheim,[11] A. J. Weinstein,[11] F. Würthwein,[11] D. M. Asner,[12] D. W. Bliss,[12] W. S. Brower,[12] G. Masek,[12] H. P. Paar,[12] J. Gronberg,[13] C. M. Korte,[13] D. J. Lange,[13] R. Kutschke,[13] S. Menary,[13] R. J. Morrison,[13] S. Nakanishi,[13] H. N. Nelson,[13] T. K. Nelson,[13] C. Qiao,[13] J. D. Richman,[13] D. Roberts,[13] A. Ryd,[13] H. Tajima,[13] M. S. Witherell,[13] R. Balest,[14] B. H. Behrens,[14] K. Cho,[14] W. T. Ford,[14] H. Park,[14] P. Rankin,[14] J. Roy,[14] J. G. Smith,[14] J. P. Alexander,[15] C. Bebek,[15] B. E. Berger,[15] K. Berkelman,[15] K. Bloom,[15] D. G. Cassel,[15] H. A. Cho,[15] D. M. Coffman,[15] D. S. Crowcroft,[15] M. Dickson,[15] P. S. Drell,[15] R. Ehrlich,[15] R. Elia,[15] A. D. Foland,[15] P. Gaidarev,[15] B. Gittelman,[15] S. W. Gray,[15] D. L. Hartill,[15] B. K. Heltsley,[15] P. I. Hopman,[15] S. L. Jones,[15] J. Kandaswamy,[15] N. Katayama,[15] P. C. Kim,[15] D. L. Kreinick,[15] T. Lee,[15] Y. Liu,[15] G. S. Ludwig,[15] J. Masui,[15] J. Mevissen,[15] N. B. Mistry,[15] C. R. Ng,[15] E. Nordberg,[15] M. Ogg,[15,†] J. R. Patterson,[15] D. Peterson,[15] D. Riley,[15] A. Soffer,[15] C. Ward,[15] P. Avery,[16] M. Athanas,[16] C. D. Jones,[16] M. Lohner,[16] C. Prescott,[16] S. Yang,[16] J. Yelton,[16] J. Zheng,[16] G. Brandenburg,[17] R. A. Briere,[17] D. Y.-J. Kim,[17] T. Liu,[17] M. Saulnier,[17] R. Wilson,[17] H. Yamamoto,[17] T. E. Browder,[18] F. Li,[18] Y. Li,[18] J. L. Rodriguez,[18] T. Bergfeld,[19] B. I. Eisenstein,[19] J. Ernst,[19] G. E. Gladding,[19] G. D. Gollin,[19] E. Johnson,[19] I. Karliner,[19] M. Palmer,[19] M. Selen,[19] J. J. Thaler,[19] K. W. Edwards,[20] A. Bellerive,[21] D. I. Britton,[21] R. Janicek,[21] D. B. MacFarlane,[21] K. W. McLean,[21] P. M. Patel,[21] A. J. Sadoff,[22] R. Ammar,[23] P. Baringer,[23] A. Bean,[23] D. Besson,[23] D. Coppage,[23] C. Darling,[23] R. Davis,[23] N. Hancock,[23] S. Kotov,[23] I. Kravchenko,[23] N. Kwak,[23] S. Anderson,[24] Y. Kubota,[24] M. Lattery,[24] J. J. O'Neill,[24] S. Patton,[24] R. Poling,[24] T. Riehle,[24] A. Smith,[24] V. Savinov,[24] M. S. Alam,[25] S. B. Athar,[25] Z. Ling,[25] A. H. Mahmood,[25] H. Severini,[25] S. Timm,[25] and F. Wappler[25]

[1]Ohio State University, Columbus, Ohio 43210
[2]University of Oklahoma, Norman, Oklahoma 73019

---

*Permanent address: BINP, RU-630090 Novosibirsk, Russia.

†Permanent address: University of Texas at Austin.

[3]Purdue University, West Lafayette, Indiana 47907
[4]University of Rochester, Rochester, New York 14627
[5]Stanford Linear Accelerator Center, Stanford University, Stanford, California 94309
[6]Southern Methodist University, Dallas, Texas 75275
[7]Syracuse University, Syracuse, New York 13244
[8]Vanderbilt University, Nashville, Tennessee 37235
[9]Virginia Polytechnic Institute and State University, Blacksburg, Virginia 24061
[10]Wayne State University, Detroit, Michigan 48202
[11]California Institute of Technology, Pasadena, California 91125
[12]University of California, San Diego, La Jolla, California 92093
[13]University of California, Santa Barbara, California 93106
[14]University of Colorado, Boulder, Colorado 80309-0390
[15]Cornell University, Ithaca, New York 14853
[16]University of Florida, Gainesville, Florida 32611
[17]Harvard University, Cambridge, Massachusetts 02138
[18]University of Hawaii at Manoa, Honolulu, Hawaii 96822
[19]University of Illinois, Champaign-Urbana, Illinois 61801
[20]Carleton University, Ottawa, Ontario, Canada K1S 5B6
and the Institute of Particle Physics, Canada
[21]McGill University, Montréal, Québec, Canada H3A 2T8
and the Institute of Particle Physics, Canada
[22]Ithaca College, Ithaca, New York 14850
[23]University of Kansas, Lawrence, Kansas 66045
[24]University of Minnesota, Minneapolis, Minnesota 55455
[25]State University of New York at Albany, Albany, New York 12222

I. INTRODUCTION

Semileptonic decays of hadrons containing a bottom quark provide a means both to measure fundamental parameters of the standard model—the magnitudes of the Cabibbo-Kobayashi-Maskawa mixing angles V_{cb} and V_{ub}—and to understand the effects of strong interactions on the underlying weak decays. These two problems are related because accurate determination of CKM elements requires a good understanding of the decay dynamics [1]. The decay $B \to D^* \ell \nu$ is a key process for these studies. From a theoretical standpoint, it has been analyzed in detail [2–12] in the framework of heavy quark effective theory (HQET), in which the decay amplitude is expanded in powers of $1/m_b$ and $1/m_c$. Because the charm and bottom masses are reasonably large compared with the energies associated with strong interactions in the decay, both the masses and the spins of the heavy quarks are expected to play little role in the dynamics. These considerations lead to symmetry relations that significantly simplify the description of the process. For $B \to D^* \ell \nu$, HQET yields numerous predictions, some of which we are able to test using the detailed studies of decay distributions presented in this paper.

In calculations of exclusive semileptonic decays, the amplitude is expressed in terms of the available four vectors (momentum and spin-polarization vectors) and one or more form factors, which are Lorentz-invariant functions that depend only on q^2, the square of the mass of the virtual W. The form factors parametrize the effect of strong interactions on the decay. Calculations of charm and bottom semileptonic decay form factors have been based on the quark model [13–18] and, more recently, on lattice QCD methods [19,20] and QCD sum rules [21–25,8]. For light charged leptons ($\ell = e$ or $\ell = \mu$), the decay $B \to D^* \ell \nu$ depends on three form factors. Although HQET does not predict their q^2 dependence, it does relate these three form factors, up to relatively small corrections, to a single universal form factor called the Isgur-Wise function. The goals of this analysis are to measure the q^2 dependence of the form factors and to test the predictions of these theoretical methods and models.

We study the form factors for $\bar{B}^0 \to D^{*+} \ell^- \bar{\nu}$ and $B^- \to D^{*0} \ell^- \bar{\nu}$ (charge-conjugate modes are implied throughout this paper) using the channels $D^{*+} \to D^0 \pi^+$ (with $D^0 \to K^- \pi^+$ or $D^0 \to K^- \pi^+ \pi^0$) and $D^{*0} \to D^0 \pi^0$ (with $D^0 \to K^- \pi^+$). The $\bar{B}^0 \to D^{*+} \ell^- \bar{\nu}$ measurement has previously been published [26]. This paper describes that measurement, a new measurement using $B^- \to D^{*0} \ell^- \bar{\nu}$, and a combined result using both decay channels.

II. DECAY DISTRIBUTIONS AND FORM FACTORS FOR $B \to D^* \ell \nu$

The differential decay rate for $B \to D^* \ell \nu$, $D^* \to D\pi$ can be expressed in terms of three q^2-dependent helicity amplitudes $H_\pm(q^2)$ and $H_0(q^2)$, where the subscripts refer to the helicity of either the virtual W or the D^*. The rate is given by

$$\frac{d\Gamma(B \to D^* \ell\nu,\ D^* \to D\pi)}{dq^2\, d\cos\theta_\ell\, d\cos\theta_V\, d\chi} = \frac{3G_F^2 |V_{cb}|^2\, P_{D^*}\, q^2}{8(4\pi)^4 m_B{}^2} \mathcal{B}(D^* \to D\pi) \times$$
$$\{[(1-\cos\theta_\ell)^2 |H_+(q^2)|^2 + (1+\cos\theta_\ell)^2 |H_-(q^2)|^2] \sin^2\theta_V$$
$$+4\sin^2\theta_\ell \cos^2\theta_V |H_0(q^2)|^2$$
$$-2\sin^2\theta_\ell \sin^2\theta_V \cos(2\chi) H_+(q^2) H_-(q^2)$$
$$-4\sin\theta_\ell (1-\cos\theta_\ell) \sin\theta_V \cos\theta_V \cos\chi\, H_+(q^2) H_0(q^2)$$
$$+4\sin\theta_\ell (1+\cos\theta_\ell) \sin\theta_V \cos\theta_V \cos\chi\, H_-(q^2) H_0(q^2)\}, \tag{1}$$

where m_B is the mass of B meson; P_{D^*} is the momentum of the D^* in the B rest frame and is a function of q^2; $\mathcal{B}(D^* \to D\pi)$ is the branching fraction for $D^{*+} \to D^0\pi^+$ or $D^{*0} \to D^0\pi^0$, as appropriate; and the angles θ_ℓ, θ_V, and χ are defined in Figure 1. Note that θ_ℓ is defined with respect to the direction of the virtual W; this accounts for the sign differences between our formula and certain others in the literature [27]. Although some of these distributions have been studied previously [28–32], our analysis is the first to use all the information from all four kinematic variables (q^2, $\cos\theta_\ell$, $\cos\theta_V$, and χ) including their correlations which provide additional information on the form factors.

The helicity amplitudes $H_\pm$ and H_0 can be expressed in terms of two axial-vector form factors, $A_1(q^2)$ and $A_2(q^2)$, and a vector form factor $V(q^2)$:

$$H_\pm(q^2) = (m_B + m_{D^*}) A_1(q^2) \mp \frac{2 m_B\, P_{D^*}}{(m_B + m_{D^*})} V(q^2),$$
$$H_0(q^2) = \frac{1}{2 m_{D^*}\sqrt{q^2}} \Big[(m_B^2 - m_{D^*}^2 - q^2)(m_B + m_{D^*}) A_1(q^2) - \frac{4 m_B^2\, P_{D^*}^2}{(m_B + m_{D^*})} A_2(q^2) \Big], \tag{2}$$

where m_{D^*} is the mass of the D^* meson. As a result of the $V-A$ coupling, the probability for producing a negative helicity D^* is larger than that for producing a positive helicity D^*, and the difference $H_-(q^2) - H_+(q^2)$ is large over much of the q^2 range.

In the heavy-quark symmetry limit ($m_c,\ m_b \to \infty$) the form factors are related to the Isgur-Wise function ξ

$$V(q^2) = A_2(q^2) = \frac{A_1(q^2)}{\left[1 - \frac{q^2}{(m_B + m_{D^*})^2}\right]} = \frac{(m_B + m_{D^*})}{2\sqrt{m_B m_{D^*}}} \xi(w), \tag{3}$$

where $w = (m_B^2 + m_{D^*}^2 - q^2)/(2 m_B m_{D^*})$. The variable w is simply the relativistic factor γ for the D^* in the B-meson rest frame, ranging from 1 to about 1.5. Following Neubert [8], we define the form factor ratios

$$R_1(w) \equiv \left[1 - \frac{q^2}{(m_B + m_{D^*})^2}\right] \frac{V(q^2)}{A_1(q^2)},$$
$$R_2(w) \equiv \left[1 - \frac{q^2}{(m_B + m_{D^*})^2}\right] \frac{A_2(q^2)}{A_1(q^2)}. \tag{4}$$

These ratios are predicted to be unity, independent of w, in the heavy-quark symmetry limit.

Because the heavy-quark symmetry limit is only an approximate description of the processes we are studying, we do not use the result given in Eq. 3 for our fits. Instead, we use general relations that do not assume infinite quark masses, but which are still appropriate to the heavy-quark effective theory expansion in that they make the infinite-mass limit easy to identify

$$\begin{aligned} A_1(q^2) &= \frac{m_B + m_{D^*}}{2\sqrt{m_B m_{D^*}}}\left[1 - \frac{q^2}{(m_B + m_{D^*})^2}\right] h_{A_1}(w), \\ A_2(q^2) &= \frac{m_B + m_{D^*}}{2\sqrt{m_B m_{D^*}}} R_2(w) h_{A_1}(w), \\ V(q^2) &= \frac{m_B + m_{D^*}}{2\sqrt{m_B m_{D^*}}} R_1(w) h_{A_1}(w). \end{aligned} \tag{5}$$

In the heavy-quark symmetry limit, $h_{A_1}(w) \to \xi(w)$, $R_1(w) \to 1$, $R_2(w) \to 1$, and Eq. 3 is recovered. We can regard the departures of R_1 and R_2 from this limit as coming from two effects: deviations of $R_1(1)$ and $R_2(1)$ from unity and a slight variation of R_1 and R_2 with w.

Although our data sample is large, we must still constrain the fit to obtain statistically meaningful results. We are able to extract three parameters, which we select based on the considerations described below. We note that previous analyses, including form factor measurements of D semileptonic decays, have extracted results on at most two parameters apart from the overall rate.

Since the range of D^* recoil velocities is rather small ($w - 1 \leq 0.5$), the form factors are expected to have approximately linear behavior. Within the framework of this assumption, the ideal fit would have five parameters: the ratios $R_1(1)$ and $R_2(1)$ and three form-factor slopes. We fit for the slope of h_{A_1}, assuming the linear form

$$h_{A_1}(w) = h_{A_1}(1)[1 - \rho^2_{A_1}(w - 1)]. \tag{6}$$

We assume that R_1 and R_2 are constant, so that the free parameters in the fit are R_1, R_2, and $\rho^2_{A_1}$. Alternative forms for h_{A_1} that have positive curvature would result in higher values of the slope at $w = 1$. Because the range of w is small, our fit is sensitive primarily to the average slope over the full w range and has little sensitivity to curvature.

In reality, R_1 and R_2 are expected to have a mild dependence on w. However, two calculations [8,12] indicate that this departure from heavy-quark symmetry is small. Since the symmetry-breaking corrections to the values of R_1 and R_2 at $w = 1$ are expected to be larger, it is more useful, with present data samples, to fit for these quantities. We will test the sensitivity of our values of R_1, R_2, and $\rho^2_{A_1}$ to this assumption by performing alternative fits in which the predicted w dependence of R_1 and R_2 is used.

In studies of charm semileptonic decay, the shapes of the form factors are usually assumed to be governed by pole forms with pole masses taken from theory. In studies of $D \to K^*\ell^+\nu$, for example, these assumptions leave two remaining parameters, quoted at $q^2 = 0$, that govern the shapes of the distributions, $r_V = V(0)/A_1(0)$ and $r_2 = A_2(0)/A_1(0)$. These differ from R_1 and R_2 which are defined to be constant in the heavy-quark symmetry limit.

It is common to report the values of certain other integrated observables that can be derived from the form factors. These are $\bar{A}_{\rm FB}$, the forward-backward asymmetry of the lepton in

the W rest frame, and $\bar{A}_{\rm pol}$, which is related to the ratio of longitudinal to transverse polarization of the D^{*+}. They are given by $\bar{A}_{\rm pol} = 2(\Gamma_L/\Gamma_T) - 1$ and $\bar{A}_{\rm FB} = 3/4(\Gamma_- - \Gamma_+)/(\Gamma_L + \Gamma_T)$, where $\Gamma_L = \Gamma_0$, $\Gamma_T = \Gamma_+ + \Gamma_-$, and $\Gamma_i = (G_F^2|V_{cb}|^2/96\pi^3) \int dq^2 P_{D^*}(q^2/{m_B}^2)|H_i(q^2)|^2$.

III. EVENT SELECTION

The data were collected using the CLEO II detector, which is described in detail elsewhere [33]. For this analysis, the most important features are the tracking system, which we use to measure charged particle momenta down to about 60 MeV/c; the CsI calorimeter, which provides excellent photon detection and electron identification; and the muon system. The integrated luminosity of the data sample is 2.4 fb^{-1} on the $\Upsilon(4S)$, which corresponds to $(2.6) \times 10^6$ $B\overline{B}$ pairs. We also use a 1.1 fb^{-1} data sample obtained at a center-of-mass energy about 60 MeV below the $\Upsilon(4S)$ to measure the continuum background.

We select events with at least one electron or muon, a reconstructed D^{*+} or D^{*0} meson, and kinematics that are consistent with a neutrino recoiling against the $D^*\ell$ system. Event selection criteria are chosen to enhance the signal over the background. The main backgrounds, starting with the largest, are from (1) combinatorial background (fake D^*'s); (2) correlated backgrounds, such as $B \to D^{**}\ell\nu$ or $B \to D^*\pi\ell\nu$ decays producing a real D^* and lepton; (3) events in which the D^* and the lepton are not from the same B meson (we call such events uncorrelated D^*-ℓ pairs because the B mesons are produced nearly at rest, leading to uncorrelated momentum vectors for the D^* and the lepton); (4) events in which a hadron has faked a lepton signature; and (5) continuum (non-$\Upsilon(4S)$ events).

We start with events satisfying the standard CLEO hadronic event criteria [34]. There is a minimum momentum requirement of 1.0 GeV/c for electron candidates and 1.4 GeV/c for muon candidates. Both electrons and muons have a maximum momentum requirement of 2.45 GeV/c for $\bar{B}^0$'s and 2.4 GeV/c for B^-'s[1]. The lepton direction must be in the range $|\cos\theta| < 0.71$, where θ is the polar angle from the beam axis. Muon candidates are identified by the presence of muon chamber hits after at least 5 nuclear interaction lengths of material. This criterion is the basis for the minimum momentum requirement of 1.4 GeV/c.

Continuum background is suppressed using an event-shape variable, R_2, equal to the ratio of the second to the zeroth Fox-Wolfram moments [35]. We require $R_2 < 0.3$, which selects events which are more more spherical and less jet-like, and which results in a continuum background that is negligible.

D^{*+}'s are reconstructed through the decay $D^{*+} \to D^0\pi^+$ using the modes $D^0 \to K^-\pi^+$ and $D^0 \to K^-\pi^+\pi^0$. In the first mode, no particle identification is required for the charged kaon and pion; besides loose track quality cuts, we require only that the candidates have opposite charges and that the kaon have the same charge as the lepton. For the three-body D decay, there is more combinatorial background, so we use dE/dx information from the drift chamber to help identify the kaon. The π^0 is identified using the CsI calorimeter: the photons are required to have energies of at least 50 MeV, the mass of the candidate

[1]The difference in cut value between the two modes is not significant, and is a result of the cuts being determined independently for the two analyses.

π^0 must be within 2σ of the nominal value [36], and the π^0 energy in the lab frame must exceed 350 MeV. The π^0 candidate is kinematically fit to the nominal π^0 mass. The kaon is required to have the same charge as the lepton. The $D^0 \to K^-\pi^+$ candidates must have a $K^-\pi^+$ mass within 16 MeV/c^2 of the known D^0 value; $D^0 \to K^-\pi^+\pi^0$ candidates must have a $K^-\pi^+\pi^0$ mass within 25 MeV/c^2 of the known value. The D^0 candidates must have a lab-frame momentum less than 2.45 GeV/c, which is close to the kinematic limit for D's from B decays.

To further reduce the combinatorial background in reconstructing the three-body D decay, we use measurements of the $D^0 \to K^-\pi^+\pi^0$ Dalitz plot from E691 [37] to compute a probability weight for each $K^-\pi^+\pi^0$ combination. We require that this weight exceed a minimum value that selects the most likely 62% of the $K^-\pi^+\pi^0$ population within the $D^0 \to K^-\pi^+\pi^0$ Dalitz plot. In events with more than one D^0 candidate, a best candidate is selected on the basis of the π^0 mass and the Dalitz amplitude.

We reconstruct charged D^* candidates by combining D^0's with additional charged tracks with a momentum of at least 65 MeV/c. The charge of this pion candidate must be opposite to that of the lepton. We select D^* candidates in both channels by requiring that the $D^* - D$ candidate mass difference δm be within 2 MeV/c^2 of the nominal value.

D^{*0}'s are reconstructed through the decay $D^{*0} \to D^0\pi^0$, with $D^0 \to K^-\pi^+$. Loose track quality cuts and dE/dx consistency are required, and the kaon candidate must have the same charge as the lepton. The $K^-\pi^+$ mass must be within 25 MeV/c^2 of the nominal D^0 mass. The slow π^0 from the D^{*0} decay is reconstructed using isolated showers in the CsI calorimeter. The showers must have an energy greater than 30 MeV, and a polar angle such that $|\cos\theta| < 0.71$. We require the π^0 candidate mass to be within 2σ of the nominal value. The showers are kinematically fit to the known π^0 mass to obtain the π^0 four momentum. The reconstructed D^{*0}'s momentum must be consistent with coming from a B decay. Finally, we require that δm be within 2 MeV/c^2 of the nominal value.

To suppress events in which the D^* and the lepton are produced in the decay chains of different B's (uncorrelated background), we require the D^* and the lepton to be in opposite hemispheres. This background arises when the lepton comes from a secondary charm decay, or a primary B decay if $B^0\bar{B}^0$ mixing has occurred. If the D^* and the lepton are produced in a $B \to D^*\ell\nu$ decay, they tend to be in opposite hemispheres, whereas the uncorrelated background is nearly uniformly distributed [38] in $\cos\theta_{D^*\ell}$, where $\theta_{D^*\ell}$ is the angle between the D^* and the lepton in the lab frame.

The final step in the event selection is designed to exploit the kinematics of the decay $B \to D^*\ell\nu$, by requiring consistency with the presence of a neutrino recoiling against the $D^*\ell^-$ system. For a signal event, we expect $p^2_{\rm miss} = p^2_\nu = 0$, where

$$\begin{aligned} p^2_{\rm miss} &= (p_B - p_{D^*\ell})^2 \\ &= m^2_B + m^2_{D^*\ell} - 2E_B E_{D^*\ell} + 2|\mathbf{p}_B||\mathbf{p}_{D^*\ell}|\cos\theta_{B,D^*\ell} \end{aligned} \tag{7}$$

and $p_{D^*\ell} = p_{D^*} + p_\ell$. Although the angle $\theta_{B,D^*\ell}$ between the B and $(D^* + \ell^-)$ momentum directions is unknown, one can neglect the last term since $|\mathbf{p}_B| \approx 330$ MeV/c is small. Thus, we define

$$M^2_{\rm miss} = m^2_B + m^2_{D^*\ell} - 2E_B E_{D^*\ell}. \tag{8}$$

The quantity $M^2_{\rm miss}$ is intuitively appealing because background from $B \to D^{**}\ell\nu$, which produces an additional pion, peaks at larger values of $M^2_{\rm miss}$ than the signal. In the D^{*+} mode, we require $M^2_{\rm miss} < 0.0$ GeV$^2/c^4$ for events with electrons and $M^2_{\rm miss} < 0.7$ GeV$^2/c^4$ for events with muons. The D^{*0} mode uses the cuts $M^2_{\rm miss} < 0.3$ GeV$^2/c^4$ for electrons and $M^2_{\rm miss} < 0.6$ GeV$^2/c^4$ for muons. The muon channel has a looser cut because the higher momentum requirement in the muon channel removes a substantial amount of the $B \to D^{**}\ell\nu$ background.

We can also impose the condition $p^2_{\rm miss} = 0$, which is satisfied for signal events, and solve Eq. 7 for $\cos\theta_{B,D^*\ell}$. The quantity $\cos\theta_{B,D^*\ell}$ computed in this way is highly correlated with the estimated value of $M^2_{\rm miss}$, but it allows us to impose the kinematic consistency condition through the requirement $|\cos\theta_{B,D^*\ell}| \leq 1$, which is satisfied by signal events up to small resolution effects. (The cut $M^2_{\rm miss} < 0$ corresponds to $\cos\theta_{B,D^*\ell} > 0$.) Figure 2 shows the δm distributions for the $D^{*+} \to D^0\pi^+$ and $D^{*0} \to D^0\pi^0$ channels, after all analysis cuts are applied except the δm cut.

	$K\pi$ e	$K\pi$ μ	$K\pi\pi^0$ e	$K\pi\pi^0$ μ	Total
Raw yield	267 ± 16	292 ± 17	192 ± 14	189 ± 14	940 ± 31
Fake D^*	17 ± 3	21 ± 4	20 ± 4	21 ± 4	79 ± 8
$B \to D^{**}\ell\nu$	12 ± 7	17 ± 8	8 ± 5	11 ± 5	48 ± 25
Uncorrelated	7 ± 4	3 ± 3	6 ± 3	0 ± 2	16 ± 6
Fake leptons	1 ± 1	6 ± 3	1 ± 1	5 ± 3	13 ± 6
Continuum	2 ± 2	3 ± 3	0 ± 2	0 ± 2	5 ± 5
Signal	228 ± 18	242 ± 20	157 ± 16	152 ± 16	779 ± 42

TABLE I. Yields for $\bar{B}^0 \to D^{*+}\ell^-\bar{\nu}$ ($D^{*+} \to D^0\pi^+$) in the $D^0 \to K^-\pi^+$ and $K\pi\pi^0$ channels and the estimated background contributions.

	$K\pi$ e	$K\pi$ μ	Total
Raw yield	376 ± 19	311 ± 18	687 ± 26
Fake D^*	123 ± 7	104 ± 7	227 ± 10
$B \to D^{**}\ell\nu$	18 ± 8	16 ± 5	34 ± 13
Uncorrelated	5 ± 8	2 ± 8	7 ± 11
Fake leptons	0 ± 2	2 ± 2	2 ± 3
Continuum	0 ± 3	0 ± 4	0 ± 6
Signal	230 ± 24	187 ± 22	417 ± 33

TABLE II. Yields for $B^- \to D^{*0}\ell^-\bar{\nu}$ ($D^{*0} \to D^0\pi^0$) in the $D^0 \to K^-\pi^+$ channel and the estimated background contributions.

IV. BACKGROUNDS

Table I and Table II lists the estimated number of events from each background and the signal in the $\bar{B}^0 \to D^{*+}\ell^-\overline{\nu}$ channels and the $B^- \to D^{*0}\ell^-\bar{\nu}$ channels respectiveley. The amount of fake D^* background under the δm peak is determined from data using the δm sideband region. The sideband region is defined as $0.15 < \delta m < 0.17$ GeV/c^2 for $\bar{B}^0$ and $0.148 < \delta m < 0.163$ GeV/c^2 for B^-. To obtain a shape for the fake D^* background in the four-dimensional fit, we use a high statistics Monte Carlo sample.

The background from $B \to D^{**}\ell\nu$, though even smaller, has a larger uncertainty, since it consists of several contributing modes that have not been well measured. Our model for these background sources is based on a combination of predictions from the model of Isgur and Scora (ISGW2) and measurements from the ALEPH experiment [39]. In the ISGW2 model [14], the dominant resonant modes contributing to $B \to D^{**}\ell\nu$ are $B \to D_1\ell^-\bar{\nu}$ and $B \to D_2^*\ell^-\bar{\nu}$, whose branching fractions are expected to be in the ratio 2:1. The D_1 and D_2^* are orbitally excited ($L = 1$) charm mesons in which the light quark and the gluons have combined spin and orbital angular momentum $j = 3/2$. The model also predicts smaller rates for decays to two other orbitally excited charm mesons, those with $j = 1/2$, only one of which decays into $D^*\pi$. Our approach is to normalize the ISGW2 model using the ALEPH [39] measurement $\mathcal{B}(b \to B)\mathcal{B}(B \to D_1^0\ell^-\bar{\nu}X)\mathcal{B}(D_1^0 \to D^{*+}\pi^-) = (2.04 \pm 0.58 \pm 0.34) \times 10^{-3}$. We assume that this rate is dominated by the resonant component $B \to D_1^0\ell^-\bar{\nu}$ to normalize the ISGW2 model. Furthermore, we add in nonresonant $B \to D^{*+}\pi^-\ell^-\bar{\nu}$ events so that the sum of all the resonant and nonresonant modes is equal to $(0.92 \pm 0.31)\%$, which we have derived from the ALEPH measurement $\mathcal{B}(b \to B)\mathcal{B}(B \to D^{*+}\pi^-\ell^-\bar{\nu}X) = (3.7 \pm 1.0 \pm 0.7) \times 10^{-3}$. The ALEPH measurements are used for consistency with the previously published form factor result [26].

Other correlated backgrounds occur when the D^* and the lepton's parent are from the same B, such as $\bar{B} \to D^*\tau^-\bar{\nu}$ or $\bar{B} \to D^*D_s^-$ and the τ or D_s decays to a lepton. These background sources are negligible.

The normalization of the uncorrelated background is determined from the data. Since this background, as described earlier, is nearly uniformly distributed in $\cos\theta_{D^*\ell}$, we use the yield of same hemisphere D^*-ℓ pairs to determine the number of opposite hemisphere uncorrelated D^*-ℓ pairs which end up in our signal region. We use Monte Carlo to model the shape of this background in our fit.

The fake lepton background is estimated using measured fake rates. The last background considered is continuum events, and is estimated using data collected below the $\Upsilon(4S)$ resonance. Both these backgrounds are small and are not included in the fit.

V. KINEMATIC VARIABLES AND ACCEPTANCE EFFECTS

To extract the form factors, we perform a fit to the joint distribution in the kinematic variables $\cos\theta_\ell$, $\cos\theta_V$, χ, and q^2. The effects of finite detector resolution and approximations used in determining these kinematic variables result in some smearing of the decay distributions. The dominant source of smearing is the unknown direction of the B meson, which has a small velocity $\beta \approx 0.06$ in the lab frame. The effects of the B motion are espe-

cially important at high q^2, where the D^* moves slowly in the B rest frame; the boost from the B motion can then account for a substantial fraction of the observed D^* momentum.

Although there is not enough information to completely determine the direction of the B momentum vector, the direction of the B meson is constrained to lie on a cone of known opening angle with respect to $\mathbf{p}_{D^*\ell}$. The azimuth of $\mathbf{p}_B$ on this cone, however, cannot be determined. Within this constraint, we consider two extreme configurations, those with the largest and smallest opening angles between $\mathbf{p}_B$ and $\mathbf{p}_{D^*}$. These configurations correspond, respectively, to the smallest and largest values of q^2 consistent with the observed four-vectors, since

$$q^2 = (p_B - p_{D^*})^2 = m_B^2 + m_{D^*}^2 - 2(E_B E_{D^*} - |\mathbf{p}_B||\mathbf{p}_{D^*}|\cos\theta_{B,D^*}). \tag{9}$$

Our method is to compute the values of q^2, $\cos\theta_\ell$, $\cos\theta_V$, and χ for each of these extreme configurations and to use the average as the estimate for each kinematic variable. Occasionally, the minimum value of q^2 will be negative, which is unphysical. In this case, we set $q^2_{\rm min} = 0$ before computing the average.

The resulting resolution in each variable is significantly improved over the calculation in which the B motion is ignored. The resolutions are q^2 dependent, with typical values $\sigma(q^2) \approx 0.5$ GeV^2/c^4, $\sigma(\cos\theta_\ell) \approx 0.07$, $\sigma(\cos\theta_V) \approx 0.07$, $\sigma(\chi) \approx 0.24$. None of these is negligible, however, and we therefore use a fitting method that takes the smearing into account.

In addition to smearing, the fit must also take into account detector acceptance. The most important acceptance effects are the poor detection efficiency for charged pions with momenta below about 100 MeV/c and the low-momentum cutoff for leptons. The soft-pion acceptance effect is particularly important at high q^2, where the D^* is moving slowly. The shape of the soft-pion acceptance has been measured in the data using $D^{*+} \to D^0\pi^+$ decays produced in continuum events. The $D^{*0} \to D^0\pi^0$ channel does not suffer severe acceptance effects for low momentum π^0's.

A similar acceptance effect arises for leptons: leptons produced in the forward direction in the W rest frame are Lorentz boosted to a higher momentum than those produced in the backward direction, for a fixed value of q^2. The cutoff in efficiency for low-momentum leptons directly affects the distribution of $\cos\theta_\ell$, since the efficiency for backward-going leptons ($\cos\theta_\ell < 0$) is very low.

VI. FITTING METHOD

The joint distribution in q^2, $\cos\theta_\ell$, $\cos\theta_V$, and χ is fit using the unbinned maximum likelihood method. To fully incorporate detector smearing and acceptance effects, we use a Monte Carlo technique [40] to evaluate the likelihood function. The likelihood of the data sample is calculated, for any given set of theoretical parameters, by computing the density of Monte Carlo events around each data point, where the Monte Carlo events are distributed according to the theoretical parameters under consideration. To avoid the need to generate separate Monte Carlo samples for every set of theoretical parameters considered by the fitter, we reweight a single Monte Carlo sample so that the weighted events give the correct density about each data point. This procedure allows us to incorporate the acceptance and smearing

effects automatically, since these are modeled by the Monte Carlo. Each channel is treated individually with their likelihoods combined for the fit.

The data is fit to a signal plus background shape. The background contains the fake D^* and uncorrelated backgrounds. The $B \to D^{**}\ell\nu$ background is treated differently. A term is not included directly in the fitting function, but we use Monte Carlo events to evaluate a small systematic shift that is caused by omitting this background in the fit. We have used ISGW2 form-factor predictions [41] to model in detail the kinematic distributions for $B \to D_1\ell^-\bar{\nu}$, $B \to D_2^*\ell^-\bar{\nu}$, and $B \to 1^{1/2}P_1\ell^-\bar{\nu}$.

VII. FIT RESULTS

We obtain fit results for the decays $\bar{B}^0 \to D^{*+}\ell^-\bar{\nu}$, $B^- \to D^{*0}\ell^-\bar{\nu}$ and a combined fit using both modes. Figure 3 shows the projections of the data and the fit in each of the four kinematic variables for the combined fit. The contribution from fake D^* and uncorrelated D^*-lepton events is shown as a dashed line.

Figures 4(a) and 4(b) show the observed distributions for $\cos\theta_V$ in the lower and upper half of the q^2 range. At low q^2, the lepton and neutrino are nearly parallel, forcing the D^* to have helicity zero; this in turn introduces a strong $\cos^2\theta_V$ component in this region of phase space. (The lack of symmetry in this variable is due to poor acceptance for very slow charged pions.) As q^2 increases, the other helicity components contribute as well, and at $q^2_{\rm max}$ the D^* must be unpolarized.

Figures 4(c) and 4(d) show an interesting correlation between $\cos\theta_V$ and χ. This correlation is produced by the interference term proportional to $(H_+(q^2) - H_-(q^2))H_0(q^2)$. The difference between H_+ and H_- results from the higher probability for the daughter c-quark to have helicity $-1/2$ than helicity $+1/2$. If the coupling at the W vertices were $(V\mp A)\times(V\pm A)$ the slopes in Figures 4(c) and 4(d) would be reversed; for $(V \pm A)(V \pm A)$ they would be the same as what we observe.

All observed distributions are described well by the fit. The values of R_1, R_2, and $\rho^2_{A_1}$ that we obtain for all three fits are given in Table III. Because there are large correlations among their errors, we also give the off-diagonal terms of the correlation matrix.

The fit results shown in Table III have been corrected by the numbers listed in the table. For the $\bar{B}^0$ mode, the corrections are due to the finite volume size used in the four-dimensional Monte Carlo likelihood calculation, and the effect of the $B \to D^{**}\ell\nu$ background. We obtain the volume size correction by fitting Monte Carlo samples and comparing measured with generated parameter values. We emphasize that the data are not binned in the likelihood fit; rather, the Monte Carlo calculation of the likelihood involves the use of discrete volume sizes around each data point. The B^- mode only requires a correction for the $B \to D^{**}\ell\nu$ background. The combined fit is corrected using the weighted average of the corrections in the individual modes. The weighted average uses the full variance matrices of the individual fits.

To test the sensitivity of the fit to the assumption that R_1 and R_2 are constants, we perform alternative fits in which we allow them to vary according to theoretical predictions of Neubert [8] and Close and Wambach [12]. Relative to our standard fit, using the Neubert prediction produces an increase in $R_1(1)$ of 0.06 and a decrease in $R_2(1)$ of 0.03, while $\rho^2_{A_1}$ is

	$B^- \to D^{*0}\ell^-\bar{\nu}$	$\bar{B}^0 \to D^{*+}\ell^-\bar{\nu}$	Combined
R_1	$1.46 \pm 0.49 \pm 0.22$	$1.18 \pm 0.30 \pm 0.12$	$1.24 \pm 0.26 \pm 0.12$
R_2	$0.82 \pm 0.33 \pm 0.11$	$0.71 \pm 0.22 \pm 0.07$	$0.72 \pm 0.18 \pm 0.07$
$\rho^2_{A_1}$	$0.98 \pm 0.22 \pm 0.07$	$0.91 \pm 0.15 \pm 0.06$	$0.92 \pm 0.12 \pm 0.06$
R_1 Correction	0.02	-0.07	-0.05
R_2 Correction	0.03	0.04	0.02
$\rho^2_{A_1}$ Correction	0.03	-0.01	-0.01
$C_{R_1 R_2}$	-0.797	-0.823	-0.814
$C_{R_1 \rho^2}$	0.634	0.612	0.618
$C_{R_2 \rho^2}$	-0.832	-0.807	-0.815

TABLE III. The fit results for both modes and the combined fit. We also list the correction applied and the correlation coefficients for the fit parameters.

essentially unchanged. With the predictions of Close and Wambach, we find an increase in $R_1(1)$ of 0.03 with $R_2(1)$ and $\rho^2_{A_1}$ unchanged. Table IV gives the results of the combined fit using these predictions, as well as fits using alternative forms for the w dependence of h_{A_1}.

The systematic errors on the fit results are given in Table V. The uncertainty in shape of the slow-pion detection efficiency as a function of momentum affects the q^2 distribution and hence primarily $\rho^2_{A_1}$. The errors on the three fit parameters are determined by reweighting the Monte Carlo events according to modified slow-pion efficiency functions. A similar reweighting procedure is performed to estimate the sensitivity to the uncertainty in lepton identification efficiency.

The uncertainty due to Monte Carlo statistics arises from the finite size of the sample used to calculate the likelihood function, and is determined by performing fits using several independent Monte Carlo samples. The correction due to finite volumes used in the likelihood function calculation was described above; the uncertainty in this correction arises from the finite Monte Carlo sample used to evaluate the correction. The finite volume systematic error for the B^- mode is dominated by the uncertainty in the effect of finite volumes on the background function.

Our fits include the uncorrelated D^{*+}–lepton background in the fitting function. The systematic error here is due to the uncertainty in the number of such events, as determined from data in the sample of events with the D^* and lepton in the same hemisphere. Finally, the fake D^* error is due to several sources: the uncertainty in the number of fake D^* events, as measured from the data sidebands; the error due to the finite Monte Carlo sample used in evaluating the likelihood; and the uncertainty in the Monte Carlo modeling of the shapes of the distributions. We have compared the kinematic distributions predicted from the fake D^* Monte Carlo with those measured from the data $D^* - D$ sideband and have found excellent agreement. We have also determined that the systematic error associated with the uncertainty on the shapes of the distributions of this background is small.

To compare with previous measurements of the lepton forward-backward asymmetry,

$h_{A_1}(w)/h_{A_1}(1)$	R_1	R_2	$\rho^2_{A_1}$
$1-\rho^2_{A_1}(w-1)$	$1.24 \pm 0.26 \pm 0.12$	$0.72 \pm 0.18 \pm 0.07$	$0.92 \pm 0.12 \pm 0.06$
$\dagger$ $1-\rho^2_{A_1}(w-1)$	$1.30 \pm 0.27 \pm 0.12$	$0.69 \pm 0.18 \pm 0.07$	$0.91 \pm 0.15 \pm 0.06$
$\ddagger$ $1-\rho^2_{A_1}(w-1)$	$1.27 \pm 0.26 \pm 0.12$	$0.72 \pm 0.18 \pm 0.07$	$0.92 \pm 0.12 \pm 0.06$
$\exp[-\rho^2_{A_1}(w-1)]$	$1.28 \pm 0.27 \pm 0.12$	$0.72 \pm 0.19 \pm 0.07$	$1.28 \pm 0.24 \pm 0.08$
$\frac{2}{w+1}\exp[(1-2\rho^2_{A_1})\frac{w-1}{w+1}]$	$1.26 \pm 0.27 \pm 0.12$	$0.74 \pm 0.18 \pm 0.07$	$1.53 \pm 0.30 \pm 0.10$
$(\frac{2}{w+1})^{2\rho^2_{A_1}}$	$1.27 \pm 0.27 \pm 0.12$	$0.73 \pm 0.18 \pm 0.07$	$1.43 \pm 0.27 \pm 0.09$
$\dagger R_1^{\rm Neub}(w) = R_1[1-0.16(w-1)+0.07(w-1)^2]$		$R_2^{\rm Neub}(w) = R_2[1+0.19(w-1)-0.05(w-1)^2]$	
$\ddagger R_1^{\rm CW}(w) = R_1[1-0.06(w-1)]$		$R_2^{\rm CW}(w) = R_2[1+0.04(w-1)]$	

TABLE IV. Combined fit results using various assumptions for $h_{A_1}(w)$, $R_1(w)$, and $R_2(w)$. The first row in the table is the standard fit with a linear form of $h_{A_1}(w)$ and constant form factor ratios. The errors on the extracted parameters are correlated as shown in Table III. The next two rows have w dependent form factor ratios according to theoretical predictions. The last three rows use alternative forms of $h_{A_1}(w)$; the extracted values of $\rho^2_{A_1}$ are sensitive to these forms. The form factor ratios are not very sensitive to the form of $h_{A_1}(w)$. The functions $R_i^{\rm Neub}(w)$ and $R_i^{\rm CW}(w)$ are taken from Refs. [8,12].

	$\bar{B}^0 \to D^{*+}\ell^-\bar{\nu}$			$B^- \to D^{*0}\ell^-\bar{\nu}$			Combined		
	δR_1	δR_2	$\delta\rho^2_{A_1}$	δR_1	δR_2	$\delta\rho^2_{A_1}$	δR_1	δR_2	$\delta\rho^2_{A_1}$
Slow pion efficiency	0.01	0.01	0.04	0.005	0.002	0.03	0.01	0.01	0.03
Finite MC statistics	0.03	0.01	0.01	0.04	0.03	0.03	0.02	0.01	0.01
Finite volumes	0.05	0.04	0.03	0.15	0.09	0.03	0.06	0.04	0.03
$B \to D^{**}\ell\nu$	0.08	0.04	0.02	0.10	0.03	0.03	0.09	0.02	0.02
Lepton efficiency	0.02	0.02	0.01	0.02	0.01	0.004	0.02	0.02	0.01
Uncorr. Background	0.03	0.01	0.01	0.09	0.03	0.01	0.03	0.01	0.01
Fake D^*	0.05	0.03	0.03	0.08	0.05	0.04	0.04	0.03	0.02
Total	0.12	0.07	0.06	0.22	0.11	0.07	0.12	0.06	0.06

TABLE V. Systematic errors on R_1, R_2, and $\rho^2_{A_1}$ for the individual fits. We combine the systematic errors from the individual fits to obtain the systematic errors quoted for the combined fit.

$\bar{A}_{\rm FB}$, and the D^* polarization, $\bar{A}_{\rm pol}$, we calculate these quantities from the result of the combined fit. We obtain $\bar{A}_{\rm FB} = 0.207 \pm 0.028 \pm 0.014$ and $\bar{A}_{\rm pol} = 1.49 \pm 0.20 \pm 0.07$, compared with the ARGUS results [28] of $\bar{A}_{\rm FB} = 0.20 \pm 0.08 \pm 0.06$ and $\bar{A}_{\rm pol} = 1.1 \pm 0.4 \pm 0.2$. For the value $\rho^2 = 0.9$, Neubert calculates [8] $\bar{A}_{\rm FB} = 0.22$ and $\bar{A}_{\rm pol} = 1.40$.

As a test of factorization, the ratio Γ_L/Γ measured in $\bar{B}^0 \to D^{*+}\rho^-$ is compared to theoretical predictions of Γ_L/Γ, at $q^2 = m_{\rho^2}$, in $B \to D^*\ell\nu$ [42]. Using our form factor measurements we calculate Γ_L/Γ, at $q^2 = m_{\rho^2}$, to be $0.911 \pm 0.013 \pm 0.006$.

VIII. CONCLUSIONS

We have measured the form factors for the decays $\bar{B}^0 \to D^{*+}\ell^-\bar{\nu}$ and $B^- \to D^{*0}\ell^-\bar{\nu}$ using an unbinned maximum likelihood fit. Three parameters are determined from the fit, two form-factor ratios R_1 and R_2, and the form-factor slope $\rho^2_{A_1}$. The q^2 dependence of each of the three form factors is assumed to be related by heavy-quark symmetry to the form factor h_{A_1}, which becomes the Isgur-Wise function in the heavy-quark symmetry limit, and which we take to be a linear function of q^2: $h_{A_1}(w) = h_{A_1}(1)[1 - \rho^2_{A_1}(w-1)]$, where w measures the D^* recoil velocity and is defined after Eq. 3.

With these assumptions, we obtain, for the combined fit, preliminary form factor ratios $R_1 = 1.24 \pm 0.26 \pm 0.12$ and $R_2 = 0.72 \pm 0.18 \pm 0.07$, which can be compared with the heavy quark symmetry limit of $R_1 = R_2 = 1$. Our values agree well with the predictions of Neubert [8], $R_1(1) = 1.35$ and $R_2(1) = 0.79$, and Close and Wambach [12], $R_1(1) = 1.15$ and $R_2(1) = 0.91$. The errors on our measurements are highly correlated, as discussed in the previous section. In the same fit, we determine the slope of $h_{A_1}(w)$ to be $\rho^2_{A_1} = 0.92 \pm 0.12 \pm 0.06$. Since we assume a linear form, this parameter measures the average slope over the w range. This value is consistent with the range 0.5 to 2.0 expected from calculations using lattice QCD and QCD sum rules. For the individual fits we obtain the results $R_1 = 1.18 \pm 0.30 \pm 0.12$, $R_2 = 0.71 \pm 0.22 \pm 0.07$, and $\rho^2_{A_1} = 0.91 \pm 0.15 \pm 0.06$ for $\bar{B}^0 \to D^{*+}\ell^-\bar{\nu}$; and $R_1 = 1.46 \pm 0.49 \pm 0.22$, $R_2 = 0.82 \pm 0.33 \pm 0.11$, and $\rho^2_{A_1} = 0.98 \pm 0.22 \pm 0.07$ for $B^- \to D^{*0}\ell^-\bar{\nu}$.

The comparison of this measurement of $\rho^2_{A_1}$ with that from the CLEO II V_{cb} measurement [32] using $B \to D^*\ell\nu$ requires some care. That measurement uses a standard procedure in which the $d\Gamma/dq^2$ distribution is fit to a function that assumes $R_1 = R_2 = 1$. For this reason, Neubert refers to the slope parameter obtained from the $d\Gamma/dq^2$ fit as $\hat{\rho}^2$. Using the relation [9]

$$\Delta\rho^2 = \hat{\rho}^2 - \rho^2_{A_1} = -\frac{1}{6}(R_1^2 - 1) - \frac{1}{3}\frac{m_B}{m_B - m_{D^*}}(1 - R_2), \tag{10}$$

we find $\rho^2_{A_1} \approx \hat{\rho}^2 + 0.24$. The CLEO II value of $\hat{\rho}^2$ is $0.84 \pm 0.13 \pm 0.08$, which would correspond to a value of $\rho^2_{A_1}$ around 1.08. Thus, the CLEO II $\rho^2_{A_1}$ and $\hat{\rho}^2$ measurements, which are essentially statistically independent, are consistent.

Our method for determining the $B \to D^*\ell\nu$ form factors is significantly different from previous studies. Earlier measurements have fit for at most two of the three parameters in our fit. Because of our large data sample and because we use the powerful information in the correlations among all the kinematic variables, we are able to fit simultaneously for all

three parameters. In the previous CLEO II measurement [30], the lepton forward-backward asymmetry $\bar{A}_{\rm FB}$ was measured, and the form factors were extracted by performing a χ^2 fit to $\bar{A}_{\rm FB}$ and to both ARGUS and CLEO measurements of $\bar{A}_{\rm pol}$ and $d\Gamma/dq^2$. In that study, the q^2 dependence of the form factors was fixed. In the ARGUS measurement [28], the quantities $\bar{A}_{\rm FB}$ and $\bar{A}_{\rm pol}$ are quoted but not the form factors. In studies [28,32,31] of the $d\Gamma/dq^2$ distribution that are used to determine $|V_{cb}|$, a slope is determined that is closely related to $\rho^2_{A_1}$. However, these measurements assume the heavy-quark symmetry limit, $R_1 = R_2 = 1$.

One of the important results of our new fit is that the corrections to the heavy-quark symmetry limit do indeed appear to be fairly small. This result provides confidence in the use of heavy-quark symmetry as a starting point for the extraction of $|V_{cb}|$ from $B \to D^* \ell \nu$. Although our study is more general than previous ones, we have still made the important assumption that the q^2 dependence of each of the three form factors can be related to a single function. Substantially more data will be required before one can allow each of the three form factors to have a separate dependence on q^2 in the fit.

We also observe a large effect produced by the interference terms in the decay amplitude, indicating a large difference in the amplitude for producing the W in helicity $+1$ and -1 states. This correlation helps to improve our measurement of R_1 and has not previously been used. The correlation is consistent with $(V-A)$ couplings at both W vertices.

ACKNOWLEDGEMENTS

We gratefully acknowledge the effort of the CESR staff in providing us with excellent luminosity and running conditions. J.P.A., J.R.P., and I.P.J.S. thank the NYI program of the NSF, M.S thanks the PFF program of the NSF, G.E. thanks the Heisenberg Foundation, K.K.G., M.S., H.N.N., T.S., and H.Y. thank the OJI program of DOE, J.R.P, K.H., and M.S. thank the A.P. Sloan Foundation, and A.W., and R.W. thank the Alexander von Humboldt Stiftung for support. This work was supported by the National Science Foundation, the U.S. Department of Energy, and the Natural Sciences and Engineering Research Council of Canada.

REFERENCES

[1] J. Richman and P. Burchat, Rev. Mod. Phys **67**, 893 (1995).
[2] N. Isgur and M.B. Wise, Phys. Lett. B **232**, 113 (1989).
[3] N. Isgur, and M.B. Wise, Phys. Lett. B **237**, 527 (1990).
[4] M.E. Luke, Phys. Lett. B **252**, 447 (1990).
[5] C.G. Boyd and D.E. Brahm, Phys. Lett. B **257**, 393 (1991).
[6] M. Neubert, Phys. Lett. B **264**, 455 (1991).
[7] M. Neubert and V. Rieckert, Nucl. Phys. B **382**, 97 (1992).
[8] M. Neubert, Phys. Reports **245**, 259 (1994).
[9] M. Neubert, Phys. Lett. B **338**, 84 (1994).
[10] T. Mannel, Phys. Rev. D **50**, 428 (1994).
[11] M. Shifman, N.G. Uraltsev, and A. Vainshtein, Phys. Rev. D **51**, 2217 (1995).
[12] F.E. Close and A. Wambach, Rutherford Lab. Preprint No. RAL-94-041 (1994).
[13] N. Isgur, D. Scora, B. Grinstein, and M.B. Wise, Phys. Rev. D **39**, 799 (1989).
[14] D. Scora and N. Isgur, CEBAF Preprint No. CEBAF-TH-94-14 (1994).
[15] J.G. Körner and G.A. Schuler, Z. Phys. C **38**, 511 (1988) [Erratum: C **41**, 690 (1989)].
[16] J.G. Körner and G.A. Schuler, Z. Phys. C **46**, 93 (1990).
[17] M. Wirbel, B. Stech, and M. Bauer, Z. Phys. C **29**, 637 (1985).
[18] M. Bauer and M. Wirbel, Z. Phys. C **42**, 671 (1989).
[19] C. Bernard, Y. Shen, and A. Soni, Phys. Lett. B **317**, 164 (1993).
[20] S.P. Booth, *et al.* (UKQCD), Phys. Rev. Lett. **72**, 462 (1994).
[21] J.D. Bjorken, in *Results and Perspectives in Physics, Proceedings of the 4th Rencontres de Physique de la Valle d'Aoste, La Thuile, Italy* ed. by M. Greco (Editions Frontières, France), p. 583 (1990); and *Proceedings of the Eighteenth SLAC Summer Institute on Particle Physics, Gauge Bosons and Heavy Quarks, July 1990,* edited by J.F. Hawthorne, SLAC-Report-378, p. 167 (1991).
[22] B. Blok and M. Shifman, Phys. Rev. D **47**, 2949 (1993).
[23] M.B. Voloshin, Phys. Rev. D **46**, 3062 (1992).
[24] H.Y. Jin, C.S. Huang, and Y.B. Dai, Z. Phys. C **56**, 707 (1992).
[25] S. Narison, Phys. Lett. B **325**, 197 (1994).
[26] J. Duboscq, *et al.* (CLEO), Phys. Rev. Lett. **76**, 3898 (1996).
[27] R.J. Morrison and J.D. Richman, "Note on Semileptonic Decays of D and B Mesons," Part I, p. 1565 and Part II, p. 1602, in *Review of Particle Properties,* Phys. Rev. D **50**, 1173 (1994).
[28] H. Albrecht *et al.* (ARGUS), Z. Phys. C **57**, 533 (1993).
[29] D. Bortoletto, *et al.* (CLEO), Phys. Rev. Lett. **63**, 1667 (1989).
[30] S. Sanghera *et al.* (CLEO), Phys. Rev. D **47**, 791 (1993).
[31] D. Buskulic *et al.* (ALEPH), Phys. Lett. B **359**, 236 (1995).
[32] B. Barish *et al.* (CLEO), Phys. Rev. D **51**, 1014 (1995).
[33] Y. Kubota *et al.* (CLEO), Nucl. Instrum. Methods A **320**, 66 (1992).
[34] Hadronic events must have at least 3 charged tracks originating near the interaction point, and the total visible energy in the calorimeter for the event must be greater than $0.15E_{\rm CM}$, where $E_{\rm CM}$ is the center-of-mass energy.
[35] G. Fox and S. Wolfram, Phys. Rev. Lett. **41,** 1581 (1978).

[36] The typical invariant mass resolution for two photons at the π^0 mass is 5-8 MeV/c^2.
[37] J.C. Anjos *et al.* (E691), Phys. Rev. D **48**, 56 (1993).
[38] In the limit that the two B mesons are produced at rest the distributions in $\cos\theta_{D^*\ell}$ is uniform. The produced B mesons from the $\Upsilon(4S)$ have a small momentum ($|\mathbf{p}_B| \approx 330$ MeV/c) which causes negligible non-uniformity in the $\cos\theta_{D^*\ell}$ distribution.
[39] D. Buskulic *et al.* (ALEPH), Phys. Lett. B **345**, 103 (1995).
[40] D.M. Schmidt, R.M. Morrison, and M. Witherell, Nucl. Instrum. Methods A **328**, 547 (1993).
[41] D. Scora and N. Isgur, Phys. Rev. D **52**, 2783 (1995).
[42] T.E.Browder and K. Honscheid, Prog. Part. Nucl. Phys. **35**, 81 (1995).

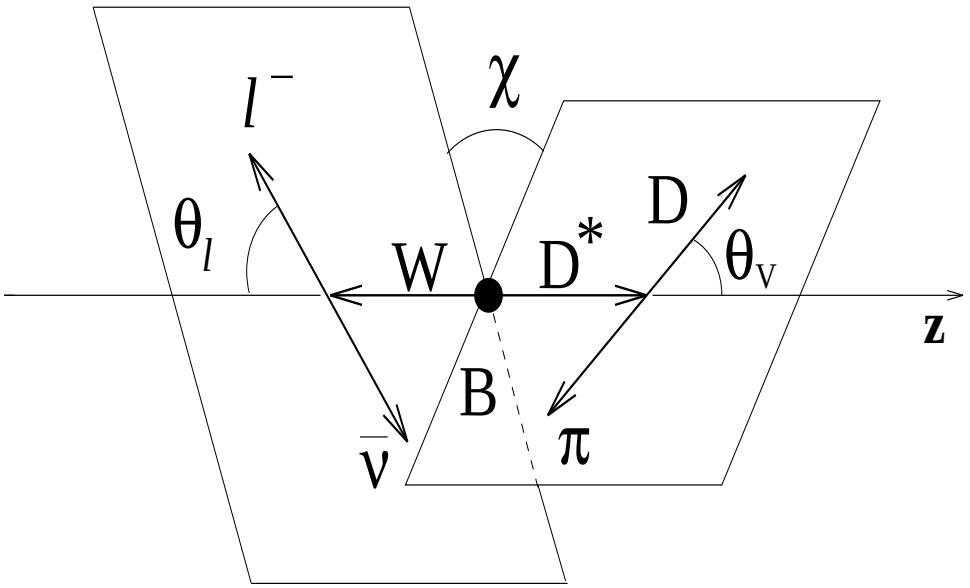

FIG. 1. Definition of the angles $\cos\theta_\ell$, $\cos\theta_V$, χ. The polar angles θ_ℓ and θ_V are defined in the rest frames of the virtual W and the D^*, respectively, and χ is the azimuthal angle between the projections of the lepton and D momentum vectors in the plane perpendicular to z.

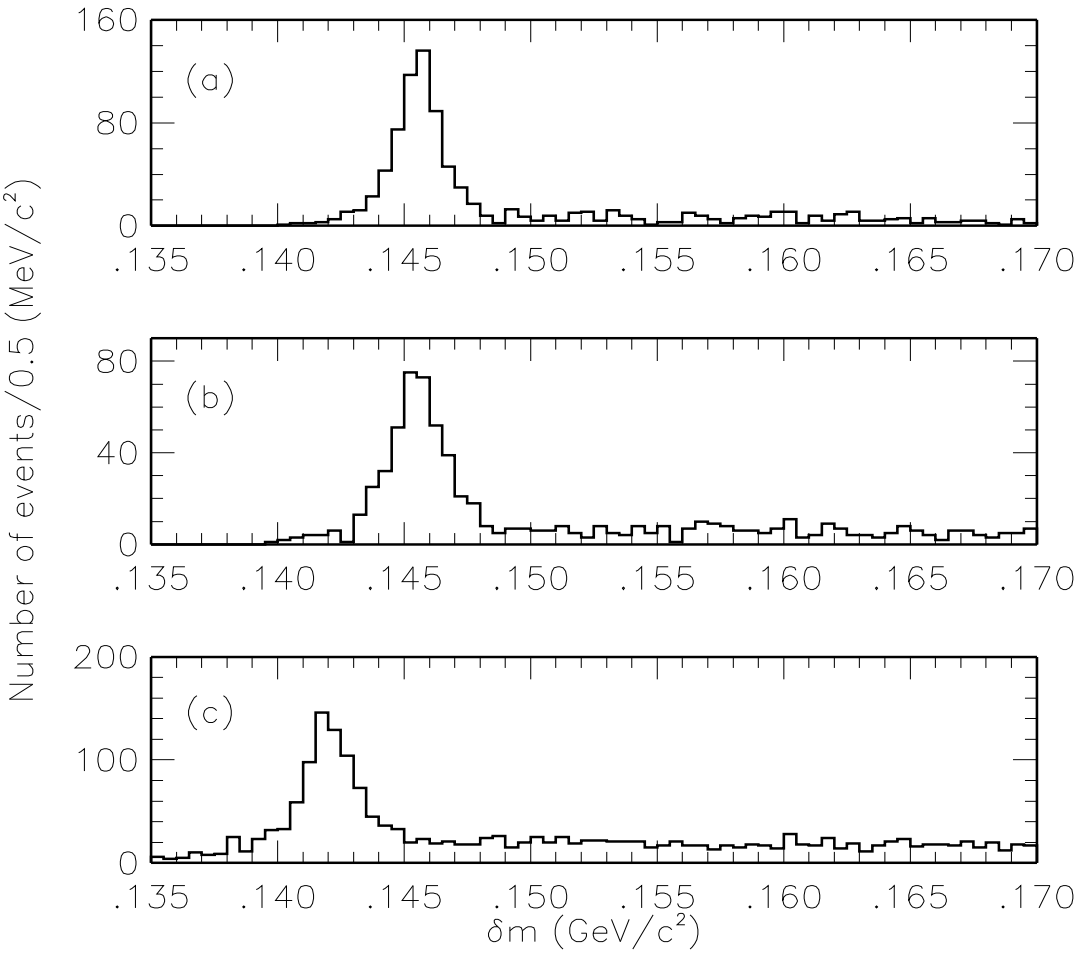

FIG. 2. The distribution of $\delta m = M(D^*) - M(D^0)$ for (a) $\bar{B}^0 \to D^{*+}\ell^-\bar{\nu}$ ($D^0 \to K^-\pi^+$), (b) $\bar{B}^0 \to D^{*+}\ell^-\bar{\nu}$ ($D^0 \to K^-\pi^+\pi^0$) and (c) $B^- \to D^{*0}\ell^-\bar{\nu}$ ($D^0 \to K^-\pi^+$) candidates after all analysis cuts except the δm cut.

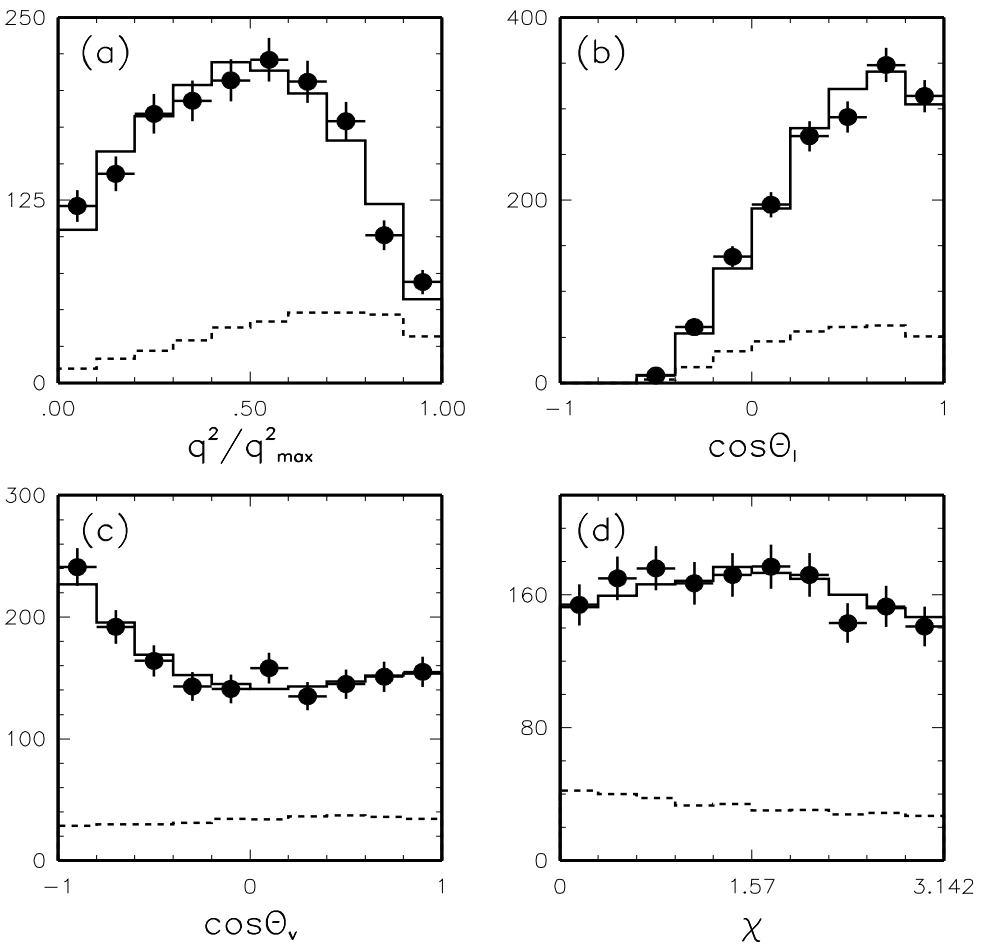

FIG. 3. The projections of the kinematic variables for the combined fit. The points with error bars are the data, and the solid histogram shows the result of the fit. The dashed line shows the contribution of the two backgrounds included in the fit: fake D^*'s and uncorrelated D^*–lepton pairs.

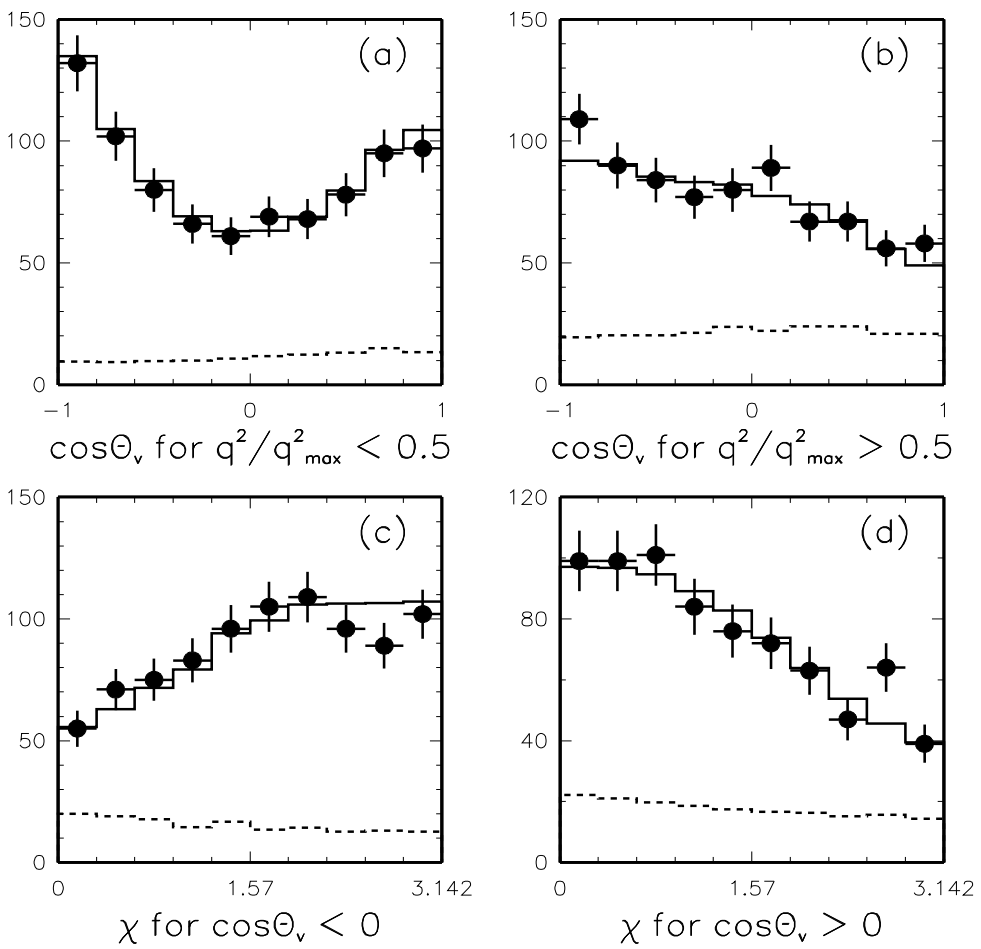

FIG. 4. Distributions of $\cos\theta_V$ for the (a) lower half and (b) upper half of the q^2 range. At low q^2, the longitudinal component of the D^* dominates. At $q^2_{\rm max}$, the D^* is unpolarized. The dotted lines in the histograms show the result of the fit, and the dashed lines show the background from fake D^*'s and uncorrelated D^*-lepton events. Figures (c) and (d) show the χ distributions for $\cos\theta_V < 0$ and $\cos\theta_V > 0$, respectively.